Ultracompact GRIN lens based spot size converter using subwavelength grating metamaterials

JOSÉ MANUEL LUQUE-GONZÁLEZ,[1*] ROBERT HALIR[1,2], J. GONZALO WANGÜEMERT-PÉREZ,[1] JOSÉ DE-OLIVA-RUBIO[1], JENS H. SCHMID[3], PAVEL CHEBEN[3], ÍÑIGO MOLINA-FERNÁNDEZ,[1,2] AND ALEJANDRO ORTEGA-MOÑUX[1]

[1]*Universidad de Málaga, Dept. de Ingeniería de Comunicaciones, ETSI Telecomunicación, Campus de Teatinos s/n, 29071 Málaga, España*
[2]*Bionand Center for Nanomedicine and Biotechnology, Parque Tecnológico de Andalucía, 29590 Málaga, Spain*
[3]*National Research Council Canada, 1200 Montreal Road, Bldg. M50, Ottawa K1A 0R6, Canada*
**Corresponding author: jmlg@uma.es*

Received XX Month XXXX; revised XX Month, XXXX; accepted XX Month XXXX; posted XX Month XXXX (Doc. ID XXXXX); published XX Month XXXX

Graded index materials offer virtually complete control over light propagation in integrated photonic chips but can be challenging to implement. Here we propose an anisotropic graded index metamaterial synthesized with fully etched silicon subwavelength structures. Based on this material, we design a spot size converter that expands the mode field from a 0.5 µm wide silicon wire waveguide to a 15 µm wide waveguide within a length of only ~14 µm. Measured insertion losses are below 1 dB in an unprecedented 130 nm bandwidth, limited by our measurement setup, with full 3D-FDTD simulations predicting a bandwidth in excess of 300 nm. We furthermore demonstrate that the device is ideally suited to feed fiber-to-chip grating couplers, with a footprint ten times shorter than conventional adiabatic tapers.

http://dx.doi.org/10.1364/OL.99.099999

1. Introduction

On chip graded index (GRIN) materials enable a plethora of different applications such as light collimation [1,2], sharp multimode bends [3,4], polarization beam splitters [5], and invisibility cloaks [6]. Such materials can be implemented either through complex grey-scale lithography or by using subwavelength gratings (SWG). A subwavelength grating is a periodic dielectric structure with a period shorter than the wavelength propagating through it, thereby enabling the synthesis of metamaterials with a controllable equivalent refractive index using a single lithographic etch step [7]. Uniform (non-graded) SWGs have been used to demonstrate myriad high-performance devices in the silicon-on-insulator (SOI) platform [8], including integrated biosensors [9], ultrabroadband waveguide couplers [10] and narrowband Bragg filters [11,12] among others. The anisotropy of such uniform SWGs has recently been exploited to achieve advanced functionalities such as broadband behavior [13], control of evanescent fields [14], and high performance polarization handling [15–17]. However, in graded index metamaterials, the advantages of this intrinsic anisotropy remain unexplored.

In this work we demonstrate the use of an anisotropic SWG based GRIN material to implement an ultracompact, robust and efficient spot size converter [see Fig. 1 (a)]. The GRIN profile is implemented by continuously changing the duty cycle of the SWG structure in the lateral direction [see Fig. 1 (b)]. We develop an anisotropic equivalent material model that shows that the anisotropy shortens the length of the device and enables a quick yet accurate way to design SWG based GRIN materials. Our lens achieves a spot size conversion from a 0.5 µm wide silicon wire to a 15 µm wide waveguide in a total length of 14 µm, making it ten times shorter than a conventional taper. Compared to other advanced spot-size converters [18–21] we achieve an unprecedented 130 nm bandwidth with measured insertion losses (IL) below 1 dB.

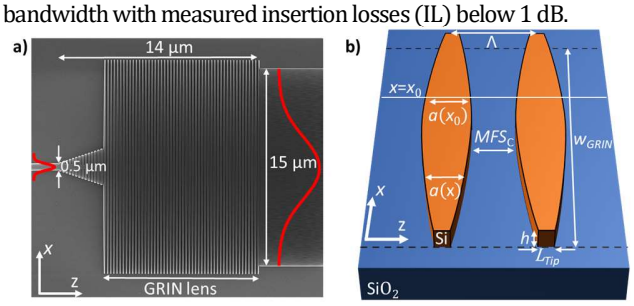

Fig. 1. a) Scanning Electron Microscope (SEM) image of the proposed spot size converter prior to the deposition of the SiO_2 cladding. The device converts the guided mode of a conventional 500nm wide silicon wire to the fundamental mode of a 15 µm wide waveguide, with insertion losses below 1 dB. b) Schematic of the subwavelength structure. The shape of the silicon blocks $a(x)$ synthesizes the required gradual index profile of the GRIN lens. The silicon dioxide cladding is not shown for clarity.

We furthermore show that the lens can be used to feed fiber-to-chip grating couplers from standard SOI waveguides with low losses. Indeed, the proposed GRIN lens SWG assisted spot size converter exhibits an exceptional combination of reduced footprint and insertion losses, as well as large bandwidth and tolerance to fabrication errors.

2. Implementing the anisotropic GRIN metamaterial

In a conventional isotropic GRIN lens, the refractive index profile follows a parabolic distribution [22]:

$$n_{GRIN}(x) = n\sqrt{1-\alpha^2 x^2}, \alpha = \frac{1}{\frac{w_{GRIN}}{2}}\sqrt{1-\left(\frac{n_{min}}{n_{max}}\right)^2}, (1)$$

where n_{max} and n_{min} are the refractive index at the center and the edges of the lens, w_{GRIN} is the width of the lens and α is a parameter which measures the curvature of the refractive index parabola. From a ray optics point of view, an isotropic GRIN lens collimates any paraxial input ray at a distance $f_{Ray} = \pi/(2\alpha)$ [22]. Therefore, the design of a compact GRIN lens-based spot size converter mainly relies on increasing the curvature of the parabola, α, to shorten the device length. However, the SWG structure exhibits an intrinsic anisotropy [15], so that the equivalent refractive index along the z-direction differs significantly from the equivalent refractive index along the x-direction. As we will show later, this does not affect the device behavior, but significantly reduces its length when compared with the isotropic case. To take the anisotropy into account, we estimate the collimation distance via electromagnetic analysis of the modes of the structure, considering the GRIN lens as a multimode gradual index waveguide. Specifically, the collimation distance can be easily derived as [23]:

$$f_{EM} = L_{\frac{\pi}{2}} = \frac{\lambda_0}{4\left(n_{eff0} - n_{eff1}\right)}, (2)$$

where n_{eff0} and n_{eff1} are the effective indices of the fundamental and first order modes respectively.

The design parameters of an SWG based GRIN lens are [see Fig. 1(b)]: i) the width of the multimode region, w_{GRIN}, which enable us to reach the desired output beam width, ii) the shape of the silicon blocks, $a(x) = DC(x)\cdot\Lambda$, which implements the required parabolic refractive index profile of the GRIN lens, and iii) the period of the structure, Λ, which optimizes the bandwidth behavior, as we will show later. First, we set $w_{\mathrm{GRIN}} = 16$ µm, only slightly wider than the desired output width to keep the curvature α as high as possible. For periods large enough to be readily fabricated, the device does not operate in the deep subwavelength regime, so that the shape $a(x)$ which synthesizes the required refractive index profile depends on the period, Λ. Hence, both parameters have to be designed simultaneously. We consider periods in the range of $\Lambda = 180$ nm to $\Lambda = 260$ nm to fulfil fabrication restrictions and avoid Bragg reflections, respectively. We now discuss the design process of the shape $a(x)$ for an intermediate period ($\Lambda = 240$ nm) and illustrate our anisotropic GRIN homogenization approach.

Our basic assumption is that the local equivalent refractive index at any position x_0 along the GRIN lens [see Fig. 1(b)], is given by the equivalent refractive index of an x-invariant SWG waveguide with the same duty cycle and period [see Fig. 2: Inset]. The core of this SWG structure can be approximated by a homogeneous anisotropic uniaxial material with permittivity tensor $\varepsilon(DC) =$

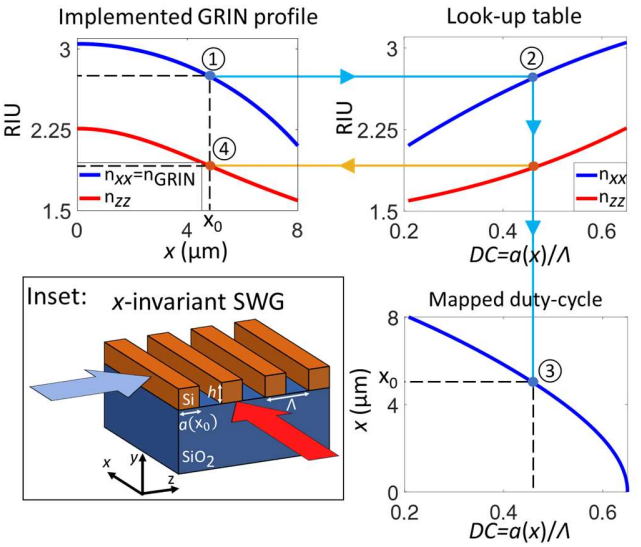

Fig. 2. To implement the equivalent refractive index $n_{xx}(x_0) = n_{GRIN}(x_0)$ at any position x_0, (marked as ①) we refer to a look-up table (marked as ②) constructed by analyzing the structure shown in the inset, obtaining the shape $a(x_0)$ (marked as ③). This in turn imposes the value of $n_{zz}(x_0)$ (marked as ④). Inset: Schematic of the periodic structure used to calculate both polarizations of the look-up table. Typical SOI values, $n_{\mathrm{Si}} = 3.476$, $n_{\mathrm{SiO2}} = 1.444$, $h = 0.22$ µm and a period $\Lambda = 0.24$ µm are assumed.

$\mathrm{diag}[n_{xx}^2(DC), n_{xx}^2(DC), n_{zz}^2(DC)]$ [15] which, for a given period, depends only on the duty cycle. Therefore, we can calculate a look-up table which maps a desired refractive index into its corresponding duty cycle as follows. First, we obtain $n_{xx}(DC)$ by computing the effective index of the fundamental x-polarized Floquet mode propagating along the z direction in the structure shown the inset of Fig. 2 (the blue arrow indicates the propagation direction). The equivalent index n_{xx} is then given by the refractive index of a homogeneous isotropic slab waveguide whose fundamental TE mode has the same effective index as the Floquet mode. Then, we obtain $n_{zz}(DC)$, by proceeding analogously with the z-polarized Floquet mode propagating along the x-axis (Fig. 2: Inset, red arrow). For illustration purposes in this figure we assume a 220 nm thick SOI platform at $\lambda_o = 1.55$ µm and, referring to Fig. 1(b), a typical tip $L_{\mathrm{Tip}} = 50$ nm on the edge of the lens and a MFS_{C} of 80 nm in the center, implying a $DC_{\mathrm{min}} = L_{\mathrm{Tip}}/\Lambda \sim 0.2$ and $DC_{\mathrm{max}} = 1 - MFS_{\mathrm{C}}/\Lambda \sim 0.65$, obtaining the look-up table shown in Fig. 2. We then impose that $n_{xx}(x)$ follow the parabolic law in Eq. (1) and use the look-up table to obtain both the shape of the silicon blocks, $a(x) = DC(x)\cdot\Lambda$, as well as the value of n_{zz} implemented by this duty cycle.

To validate our model, we compare 3D-FDTD simulations of the periodic lens structure [Fig. 3(a)] with a homogenous anisotropic lens [Fig. 3(b)] and a homogenous isotropic lens [Fig. 3(c)], when they are illuminated by 3×0.22 µm^2 (width by height) gaussian beam. In the periodic lens structure the periods are shaped as determined by the algorithm presented in Fig. 2. In Fig. 3 we have indicated with a black dashed line the distance where the beams have been fully expanded and collimated. Three important conclusions can be drawn from Fig. 3: i) the proposed structure works as a spot size converter [Fig. 3(a)], ii) it can be accurately homogenized as an anisotropic graded index metamaterial

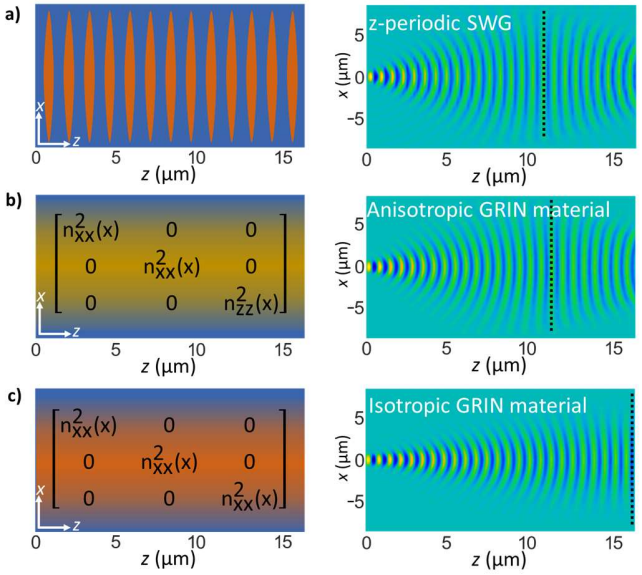

Fig. 3. Schematic of the structure (left) and real part of the main component of the electric field propagation, $\mathcal{R}e\{E_x(x,z)\}$, along the proposed GRIN lens (right) implemented with a) a z-periodic SWG structure, b) a gradual anisotropic material and c) a gradual isotropic material.

[compare Fig. 3(a) and Fig. 3(b)], iii) the isotropic homogenization does not emulate the z-periodic structure behavior [compare Fig. 3(a) and Fig. 3(c)]. Note that the formula $f_{Ray} = \pi/(2\alpha)$, with α as defined in Eq. 1, predicts a 17 μm collimation distance for the isotropic approach, close to the simulated isotropic value. Otherwise, the collimation distance is accurately predicted by computing the effective indexes of the two lowest order modes of the gradual anisotropic waveguide [Fig. 3(b)] and applying Eq. (2), yielding 12 μm collimation distance, very close to the 11 μm of the periodic structure. Therefore, the anisotropic model can be used to design the proposed GRIN lens with an anisotropic mode solver which is much faster than 3D-FDTD simulations.

3. Numerical optimization of the GRIN lens spot size converter

We now design the shape of the silicon blocks $a(x)$ using the anisotropic model exposed in the previous section to seek a short, robust and broadband GRIN lens. Figure 4(a) shows the collimation distance as a function of the minimum feature size in the center of the lens $MFS_C = (1 - DC_{\max})\Lambda$ for different periods in the range $\Lambda = 180$ nm to $\Lambda = 260$ nm. In these simulations, we fixed the lens width $w_{GRIN} = 16$ μm and the tip length $L_{Tip} = DC_{\min}\Lambda = 50$ nm [see Fig. 1(b)], i.e. we maintained $n_{\min}$ while changing $n_{\max}$. Note that each value of MFS_C implies a different refractive index profile $n_{GRIN}(x)$, and therefore also a different shape of the silicon blocks $a(x)$ [see Fig. 4(a): Inset]. This calculation has been carried out by using the proposed anisotropic GRIN model to calculate the modes of the multimode gradual index anisotropic waveguide and then applying Eq. (2) to estimate the collimation distance. Figure 4(a) reveals that the minimum collimation distance, marked with a dot for each period, is not achieved when the ratio $n_{\max}/n_{\min}$ is maximum ($DC_{\max} = 1 \rightarrow MFS_C = 0$) as would be the case in an isotropic GRIN lens [see Eq (1)]. This behavior is auspicious because it implies that the optimum MFS_C for a shorter device depends on

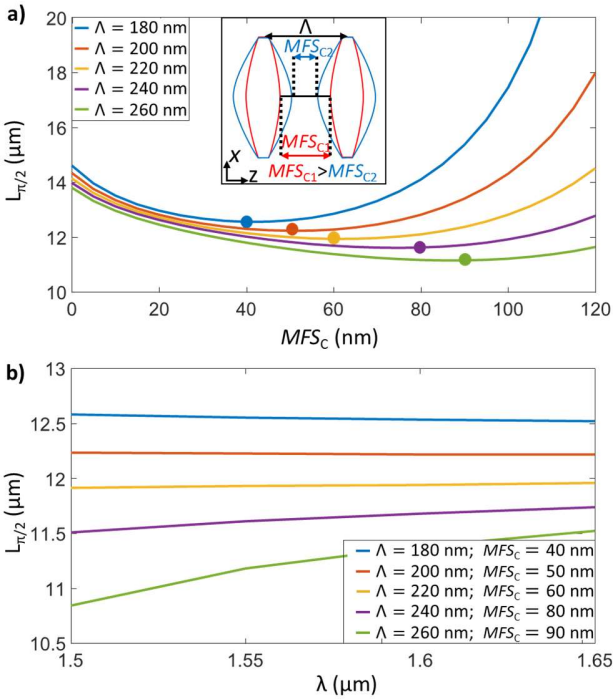

Fig. 4. a) Collimation distance as a function of the gap in the center of the lens (MFS_C) calculated for different periods as obtained through modal analysis of the homogenized anisotropic structure. Inset: Schematic of the period shape variation when changing the MFS_C maintaining w_{GRIN} and L_{Tip}. b) Collimation distance dispersion assuming the optimum MFS_C for each period (marked with solid circles in Fig. 4a)).

the period and it is in the range of 50-90 nm. A flatter curve around the design point in Fig. 4(a) indicates that the device will be more tolerant to fabrication errors. We then calculate the wavelength dependence of the collimation distance assuming its optimum MFS_C for each period [see Fig. 4(b)]. Longer pitches imply a shorter collimation distance, but the response of the device is more dispersive at short wavelengths because of the proximity to the Bragg regime. Therefore, from Fig. 4(a) and 4(b) we conclude that the period should be fixed to 240 nm with a minimum feature size $MFS_C \sim 80$ nm in the center, achieving a flat dispersion behavior with a fabricable MFS. As shown in Fig. 1(a), the lens is excited via a short (15 periods long) taper which has a dual purpose: i) it provides index matching between the 500 nm wide silicon wire waveguide and the subwavelength structure, ii) it slightly expands the mode field profile from the input waveguide to ~ 2.5 μm, exciting fewer high order modes in the lens. Finally, we refine the length of the GRIN lens via 3D-FDTD simulations, obtaining a final lens length of 10.5 μm, just 1 μm shorter than the anisotropic estimation. Final device dimensions are summarized in Table I. In Fig. 5(b) we show the simulated IL of the resulting spot size converter, achieving IL<1 dB in a bandwidth in excess of 300 nm.

GRIN lens	$w_{GRIN} = 16$ μm $L_{Tip} = 50$ nm $MFS_C = 80$ nm	$\Lambda = 240$ nm $a(x)$: see Fig. 2 # periods= 44
Input taper	$\Lambda = 240$ nm $w_{inTaper} = 0.5$ μm # periods= 15	$DC = 0.65$ $w_{OutTaper} = 2.5$ μm

Table I. Geometrical parameters of the proposed spot size converter.

4. Fabrication and Characterization

In order to experimentally demonstrate the proposed structure, a collection of GRIN lens SWG assisted spot size converters has been fabricated in a 220 nm thick SOI platform. The buried oxide (BOX) and the upper SiO_2 cladding are 2 µm and 2.2 µm thick respectively [24]. The designed spot size converter has been fabricated with the nominal parameters [Table I] and $\pm 10\%$ duty cycle offsets to study the robustness of the device. We implemented a set of back to back lenses cascaded multiple times to obtain the insertion losses of one GRIN lens (cutback configuration).

Light from a tunable laser (Agilent 81600B) connected to a lensed polarization maintaining fiber (PMF) is coupled into the chip using an SWG edge coupler [25]. The PMF is mounted on a rotatory mount, which, together with a Glan-Thompson polarizer at the output allows us to control the polarization on the chip. At the chip output, light is focused onto a photodetector (818-IR) using a microscope objective. The transmission spectrum is measured by sweeping the wavelength of the tunable laser while recording the output power. Figure 5(a) shows the normalized measured output power at the central wavelength of the measured band ($\lambda = 1.58$ µm) as a function of the number of cascaded lenses. Note that less than 1 dB insertion losses are attained even with a $\pm 10\%$ offset in the duty cycle, indicating a good tolerance to fabrication deviations. Figure 5(b) draws the simulated (dashed blue line) and measured (solid blue line) insertion losses of the nominal SWG GRIN lens spot size converter; spurious reflections have been removed using the minimum phase technique [26]. From this setup we conclude that the device shows an excellent performance in terms of: i) insertion losses, with IL<0.6 dB at the central wavelength, ii) bandwidth, with IL<1 dB from 1.51 to 1.64 µm limited by our setup, extending beyond 1.8 µm in simulation. In table II we summarize the main characteristic of state-of-the-art spot-size-converters (SSC) in the SOI platform. To compare different expansion ratios, ($ER = w_{out}/w_{in}$), we use the Normalized Expansion Ratio (NER) [20]

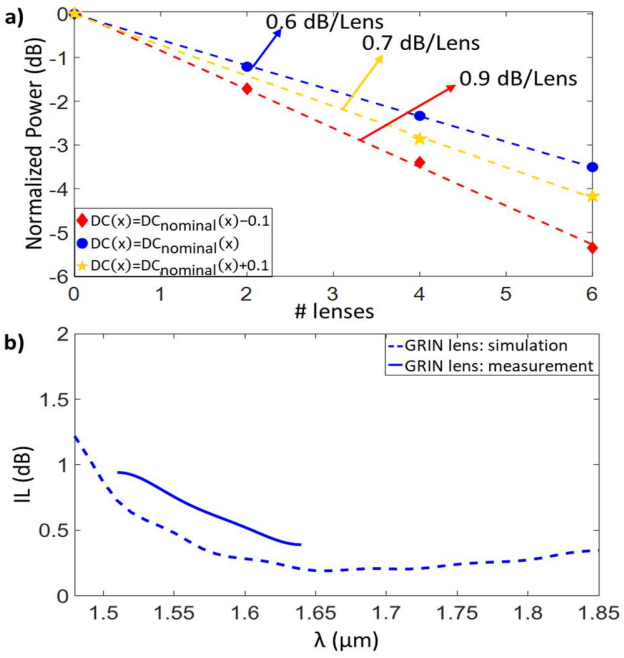

Fig. 5. a) Measured transmitted power as a function of the number of GRIN lenses at $\lambda = 1.58$ µm. Three different structures have been characterized: the nominal design and two lenses with duty cycle offsets of $\pm 10\%$ respectively. b) Insertion Losses as a function of the wavelength for the nominal SWG lens design (blue lines). Measurements were performed using a back to back configuration, so measured insertion losses are divided by two. Our Measurement setup is limited to the 1.51 µm $< \lambda <$ 1.64 µm wavelength range.

$$NER(\lambda) = \frac{w_{out}/w_{in}}{L/\lambda} \cdot IL(\lambda), (3)$$

where w_{out} and w_{in} are the widths of the output and input waveguides, L is the length of the spot size converter, λ is the wavelength of the propagating light and IL are the device insertion losses in linear scale. Our lens provides an excellent NER over an extremely broad bandwidth compared to the state-of-the-art.

Structure	IL (dB)	BW (nm)	ER	L (µm)	NER (λ_0)	Ref.
Seg. Taper	<1	50	24	20	1.86	[18]
Adiabatic Taper	<1	N/A	24	150	0.24	[19]
Semi Lens	<1	50	20	10	2.85	[20]
Hollow Taper	1.4*	43*	50*	60*	0.9*	[21]
This work	<1	130	30	15	2.90	-

Table II. Performance of some state-of-the-art spot size converters (*Simulation results).

As a further validation, we have used our spot size converter to feed a pair of grating couplers in a back to back configuration [see Fig. 6(a) and Fig. 6(b): Inset]. In this case, the measurement setup changes slightly: light from the laser is now coupled into a conventional SMF-28 fiber and the polarization is set to the desired TE state using a polarization controller (Agilent 8169A). To measure the output level, a power meter has been used (Agilent 81634B). Figure 6(b) compares the measured power when gratings are fed with a 150 µm linear taper and with the proposed spot size converters. The designed GRIN lens shows a similar behavior in terms of insertion losses that the linear 150 µm taper even with a grating coupler which has been designed to be coupled from a conventional waveguide and not for a GRIN lens. For the nominal GRIN lens, we observed comparatively high back-reflections of 14% due to the index mismatch between the lens and the grating. The back-reflections can be decreased by adding a properly designed transition between the GRIN lens and the grating coupler [27]. In this case, the +15% duty cycle offset GRIN lens yields a reduction of back-reflections to 8%, without significant impact on insertion losses.

4. Conclusion

In conclusion, we have reported a compact spot size converter based on an anisotropic GRIN lens implemented via a SWG structure. The proposed device expands the field profile thirty times (from a 0.5 µm width silicon wire to a 15 µm width waveguide) over a distance of only 14 µm with IL under 1 dB in a measured bandwidth of 130 nm, while simulation predicts a bandwidth in excess of 300 nm. Compared with state-of-the-art devices, our lens

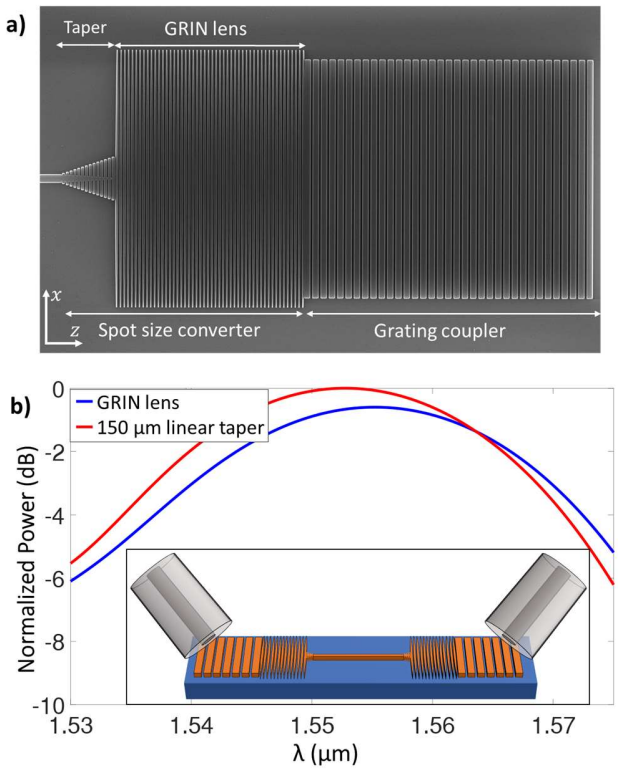

Fig. 6. a) SEM image of the transition from a conventional 0.5 μm width silicon wire to a 15 μm width grating coupler, through the proposed GRIN lens spot size converter. b) Measured wavelength response of a surface grating coupler fed with: i) a conventional 150 μm length linear taper (red line) and ii) the proposed GRIN lens expander (blue line). The curves have been normalized to the maximum coupling efficiency of the 150 μm length linear taper fed grating structure to facilitate the comparison. Inset: Schematic of the back to back grating coupler configuration when feeding with a pair of the proposed GRIN lens spot size converters.

achieves an excellent expansion ratio with outstanding bandwidth and robustness to fabrication errors. The device has been proposed to feed a grating coupler with compelling results. Moreover, the anisotropic homogenization model proposed enables fast yet accurately simulations of the GRIN metamaterial. We believe that this methodology opens up new routes for on-chip light handling.

FUNDING

We acknowledge funding from: Universidad de Málaga; Ministerio de Economía y Competitividad (MINECO) (TEC2016-80718-R); Ministerio de Educación, Cultura y Deporte (MECD) (FPU16/06762); Fondo Europeo de Desarrollo Regional—FEDER;

Reference

1. U. Levy, M. Abashin, K. Ikeda, A. Krishnamoorthy, J. Cunningham, and Y. Fainman, "Inhomogenous Dielectric Metamaterials with Space-Variant Polarizability," Phys. Rev. Lett. **98**, 243901 (2007).
2. Q. Wu, J. P. Turpin, and D. H. Werner, "Integrated photonic systems based on transformation optics enabled gradient index devices," Light Sci. Appl. **1**, e38 (2012).
3. L. H. Gabrielli, D. Liu, S. G. Johnson, and M. Lipson, "On-chip transformation optics for multimode waveguide bends," Nat. Commun. **3**, 1216–1217 (2012).
4. H. Xu and Y. Shi, "Ultra-Sharp Multi-Mode Waveguide Bending Assisted with Metamaterial-Based Mode Converters," Laser Photon. Rev. **12**, 1700240 (2018).
5. P. A. Teixeira, D. G. Silva, L. H. Gabrielli, D. H. Spadoti, and M. A. F. C. Junqueira, "General multimode polarization splitter design in uniaxial media," Opt. Eng. **57**, 1 (2018).
6. J. Li and J. B. Pendry, "Hiding under the carpet: A new strategy for cloaking," Phys. Rev. Lett. **101**, 1–4 (2008).
7. P. Cheben, R. Halir, J. H. Schmid, H. A. Atwater, and D. R. Smith, "Subwavelength integrated photonics," Nature **560**, 565–572 (2018).
8. R. Halir, A. Ortega-Monux, D. Benedikovic, G. Z. Mashanovich, J. G. Wanguemert-Perez, J. H. Schmid, I. Molina-Fernandez, and P. Cheben, "Subwavelength-Grating Metamaterial Structures for Silicon Photonic Devices," Proc. IEEE **106**, 2144–2157 (2018).
9. L. Torrijos-Morán and J. García-Rupérez, "Single-channel bimodal interferometric sensor using subwavelength structures," Opt. Express **27**, 8168–8179 (2019).
10. H. Yun, L. Chrostowski, and N. A. F. Jaeger, "Ultra-broadband 2 × 2 adiabatic 3 dB coupler using subwavelength-grating-assisted silicon-on-insulator strip waveguides," Opt. Lett. **43**, 1935–1938 (2018).
11. J. Čtyroký, J. G. Wangüemert-Pérez, P. Kwiecien, J. Litvik, J. H. Schmid, Í. Molina-Fernández, A. Ortega-Moñux, M. Dado, and P. Cheben, "Design of narrowband Bragg spectral filters in subwavelength grating metamaterial waveguides," Opt. Express **26**, 3041–3044 (2018).
12. P. Cheben, J. Čtyroký, J. H. Schmid, S. Wang, J. Lapointe, J. G. Wangüemert-Pérez, Í. Molina-Fernández, A. Ortega-Moñux, R. Halir, D. Melati, D. Xu, S. Janz, and M. Dado, "Bragg filter bandwidth engineering in subwavelength grating metamaterial waveguides," Opt. Lett. **44**, 1043–1046 (2019).
13. R. Halir, P. Cheben, J. M. Luque-González, J. D. Sarmiento-Merenguel, J. H. Schmid, G. Wangüemert-Pérez, D.-X. Xu, S. Wang, A. Ortega-Moñux, and Í. Molina-Fernández, "Ultra-broadband nanophotonic beamsplitter using an anisotropic sub-wavelength metamaterial," Laser Photon. Rev. **10**, 1039–1046 (2016).
14. S. Jahani, S. Kim, J. Atkinson, J. C. Wirth, F. Kalhor, A. Al Noman, W. D. Newman, P. Shekhar, K. Han, V. Van, R. G. DeCorby, L. Chrostowski, M. Qi, and Z. Jacob, "Controlling evanescent waves using silicon photonic all-dielectric metamaterials for dense integration," Nat. Commun. **9**, 1893 (2018).
15. J. M. Luque-González, A. Herrero-Bermello, A. Ortega-Moñux, Í. Molina-Fernández, A. V. Velasco, P. Cheben, J. H. Schmid, S. Wang, and R. Halir, "Tilted subwavelength gratings: controlling anisotropy in metamaterial nanophotonic waveguides," Opt. Lett. **43**, 4691–4694 (2018).
16. H. Xu, D. Dai, and Y. Shi, "Ultra-Broadband and Ultra-Compact On-Chip Silicon Polarization Beam Splitter by Using Hetero-Anisotropic Metamaterials," Laser Photonics Rev. **1800349**, 1–7 (2019).
17. A. Herrero Bermello, J. M. Luque Gonzalez, A. Velasco, A. Ortega-Monux, P. Cheben, and R. Halir, "Design of a broadband polarization splitter based on anisotropy-engineered tilted subwavelength gratings," IEEE Photonics J. **11**, 1–8 (2019).
18. J. Zou, Y. Yu, M. Ye, L. Liu, S. Deng, X. Xu, and X. Zhang, "Short and efficient mode-size converter designed by segmented-stepwise method," Opt. Lett. **39**, 6273–6276 (2014).
19. Y. Fu, T. Ye, W. Tang, and T. Chu, "Efficient adiabatic silicon-on-insulator waveguide taper," Photonics Res. **2**, A41 (2014).
20. S. Abbaslou, R. Gatdula, M. Lu, A. Stein, and W. Jiang, "Ultra-short beam expander with segmented curvature control: the emergence of a semi-lens," Opt. Lett. **42**, 4383–4386 (2017).
21. M. Asaduzzaman, M. Bakaul, E. Skafidas, and M. R. H. Khandokar, "A compact silicon grating coupler based on hollow tapered spot-size converter," Sci. Rep. **8**, 2540 (2018).
22. B. E. A. Saleh and M. C. Teich, *Fundamentals of Photonics*, Wiley Series in Pure and Applied Optics (John Wiley & Sons, Inc., 1991).
23. S. El-Sabban and D. Khalil, "Multimode waveguide spot size width

converter for silicon photonics applications," Opt. Eng. **54**, 037103 (2015).
24. "Applied Nanotools Inc. Canada," https://www.appliednt.com/nanosoi/.
25. P. Cheben, D.-X. Xu, S. Janz, and A. Densmore, "Subwavelength waveguide grating for mode conversion and light coupling in integrated optics," Opt. Express **14**, 4695–4702 (2006).
26. R. Halir, Í. Molina-Fernández, J. G. Wangüemert-Pérez, A. Ortega-Moñux, J. De-Oliva-Rubio, and P. Cheben, "Characterization of integrated photonic devices with minimum phase technique," Opt. Express **17**, 8349–8361 (2009).
27. D. Benedikovic, C. Alonso-Ramos, D. Pérez-Galacho, S. Guerber, V. Vakarin, G. Marcaud, X. Le Roux, E. Cassan, D. Marris-Morini, P. Cheben, F. Boeuf, C. Baudot, and L. Vivien, "L-shaped fiber-chip grating couplers with high directionality and low reflectivity fabricated with deep-UV lithography," Opt. Lett. **42**, 3439–3442 (2017).